Hearing Research 319 (2015) 56–68

Contents lists available at ScienceDirect

Hearing Research

journal homepage: www.elsevier.com/locate/heares

Research paper

Familial hemiplegic migraine type-1 mutated $Ca_V2.1$ calcium channels alter inhibitory and excitatory synaptic transmission in the lateral superior olive of mice

Carlota González Inchauspe [a, *, 1], Nadia Pilati [b, 1, 2], Mariano N. Di Guilmi [a], Francisco J. Urbano [a], Michel D. Ferrari [c], Arn M.J.M. van den Maagdenberg [c, d], Ian D. Forsythe [b], Osvaldo D. Uchitel [a]

[a] Instituto de Fisiología, Biología molecular y Neurociencias, CONICET, Departamento de Fisiología, Biología Molecular y Celular, Facultad de Ciencias Exactas y Naturales, Universidad de Buenos Aires, Argentina
[b] Dept Cell Physiology & Pharmacology, University of Leicester, LE1 9HN, UK
[c] Department of Neurology, Leiden University Medical Centre, P.O. Box 9600, 2300 RC Leiden, The Netherlands
[d] Department of Human Genetics, Leiden University Medical Centre, P.O. Box 9600, 2300 RC Leiden, The Netherlands

ARTICLE INFO

Article history:
Received 13 February 2014
Received in revised form
11 November 2014
Accepted 21 November 2014
Available online 4 December 2014

ABSTRACT

$Ca_V2.1$ Ca^{2+} channels play a key role in triggering neurotransmitter release and mediating synaptic transmission. Familial hemiplegic migraine type-1 (FHM-1) is caused by missense mutations in the *CACNA1A* gene that encodes the α_{1A} pore-forming subunit of $Ca_V2.1$ Ca^{2+} channels. We used knock-in (KI) transgenic mice harbouring the pathogenic FHM-1 mutation R192Q to study inhibitory and excitatory neurotransmission in the principle neurons of the lateral superior olive (LSO) in the auditory brainstem. We tested if the R192Q FHM-1 mutation differentially affects excitatory and inhibitory synaptic transmission, disturbing the normal balance between excitation and inhibition in this nucleus. Whole cell patch-clamp was used to measure neurotransmitter elicited excitatory (EPSCs) and inhibitory (IPSCs) postsynaptic currents in wild-type (WT) and R192Q KI mice. Our results showed that the FHM-1 mutation in $Ca_V2.1$ channels has multiple effects. Evoked EPSC amplitudes were smaller whereas evoked and miniature IPSC amplitudes were larger in R192Q KI compared to WT mice. In addition, in R192Q KI mice, the release probability was enhanced compared to WT, at both inhibitory (0.53 ± 0.02 *vs.* 0.44 ± 0.01, $P = 2.10^{-5}$, Student's *t*-test) and excitatory synapses (0.60 ± 0.03 *vs.* 0.45 ± 0.02, $P = 4\ 10^{-6}$, Student's *t*-test). Vesicle pool size was diminished in R192Q KI mice compared to WT mice (68 ± 6 vs 91 ± 7, $P = 0.008$, inhibitory; 104 ± 13 vs 335 ± 30, $P = 10^{-6}$, excitatory, Student's *t*-test). R192Q KI mice present enhanced short-term plasticity. Repetitive stimulation of the afferent axons caused short-term depression (STD) of E/IPSCs that recovered significantly faster in R192Q KI mice compared to WT. This supports the hypothesis of a gain-of-function of the $Ca_V2.1$ channels in R192Q KI mice, which alters the balance of excitatory/inhibitory inputs and could also have implications in the altered cortical excitability responsible for FHM pathology.

1. Introduction

Transmitter release in mammalian central and peripheral synapses is triggered by Ca^{2+} influx through voltage-activated Ca^{2+} channels (VACCs). Presynaptic calcium channel types undergo developmental changes during the time course of maturation. There is a decline of N-type channel density (sensitive to ω-conotoxin GVIA Ca^{2+} channel blocker) at the same time as an increase of P/Q-type ($Ca_V2.1$) channel density (sensitive to ω-Agatoxin IVA)

* Corresponding author. Facultad de Ciencias Exactas y Naturales, Pabellon II piso 2, Ciudad Universitaria, Buenos Aires 1428, Argentina. Fax: +54 11 4576 3321.
E-mail addresses: carlota@fbmc.fcen.uba.ar (C.G. Inchauspe), nadia.pilati@autifony.com (N. Pilati).
[1] CGI and NP contributed equally to this work.
[2] Current address: Autifony S.r.l. Via Fleming 4, 37135 Verona (VR), Italy.

http://dx.doi.org/10.1016/j.heares.2014.11.006
0378-5955/

at the membrane of presynaptic nerve terminals (Iwasaki and Takahashi, 1998; Iwasaki et al., 2000; Fedchyshyn and Wang, 2005; Rosato Siri and Uchitel, 1999; Rosato Siri et al., 2002; Urbano et al., 2002). It is now accepted that in adult animals, $Ca_V2.1$ Ca^{2+} channels are most efficient to trigger vesicular fusion and transmitter release at a large subset of synapses, while other synapses are mediated synergistically by multiple types of Ca^{2+} channels (Giugovaz-Tropper et al., 2011; Qian and Noebels, 2000; Mintz et al., 1995; Wu et al., 1999; Cao et al., 2004; Brown et al., 2004; Cao and Tsien, 2010; Tottene et al., 2009; Takahashi and Momiyama, 1993; Luebke et al., 1993).

Several human channelopathies result from mutations in the α_{1A} pore-forming subunit of $Ca_V2.1$ Ca^{2+} channels. $Ca_V2.1$ channels are expressed in all brain structures that have been implicated in the pathogenesis of migraine, including the cerebral cortex, the trigeminal ganglia, and brainstem nuclei involved in the central control of nociception. Familial hemiplegic migraine type 1 (FHM-1) is a Mendelian subtype of migraine with aura that is caused by missense mutations in the *CACNA1A* gene that encodes this α_{1A} subunit (Pietrobon, 2005, 2010; Ophoff et al., 1996; Vecchia and Pietrobon, 2012). Typical migraine attacks in FHM patients are associated with transient hemiparesis and are a useful model to study pathogenic mechanisms of the common forms of migraine (Ferrari et al., 2008). Current evidence indicates that cortical spreading depression (CSD) is the primary event in activating the trigeminovascular system in migraine with aura and, perhaps, also migraine without aura. An alternative hypothesis suggests that migraine headache arises from a dysfunction within the subcortical brainstem that modulates trigeminal nociceptive inputs (Akerman et al., 2011; Pietrobon and Striessnig, 2003; Sanchez del Rio and Alvarez Linera, 2004; Sanchez-del-Rio and Reuter, 2004). This latter hypothesis considers migraine aura and headache as parallel rather than sequential processes, and proposes that the primary cause of migraine headache is an episodic dysfunction in brainstem nuclei that are involved in the central control of nociception and might exert a permissive role by favoring central trigeminal hyperexcitability (Cao et al., 2002; Weiller et al., 1995; Bahra et al., 2001 May and Goadsby, 1999; Goadsby et al., 2002). Migraine patients show enhanced sensitivity to light and sound compared to healthy controls (Main et al., 1997) and dysfunction of brainstem medial olivocochlear systems are linked to phonophobia symptoms associated with migraine headache (Bolay et al., 2008). Therefore we also believe that, studying synaptic transmission within a nucleus of the brainstem could provide information relevant to neuronal circuits affected in migraine.

The generation of two knock-in (KI) FHM-1 mouse models carrying either the human pathogenic R192Q or S218L missense mutations allowed the first analysis of the functional consequences of FHM-1 mutations on $Ca_V2.1$ channels and synaptic transmission in neurons expressing the channels at the endogenous physiological level (van den Maagdenberg et al., 2010, 2007, 2004; Kaja et al., 2010; Tottene et al., 2009; González Inchauspe et al., 2010; Adams et al., 2010). In agreement with the hypothesis that considers CSD as the underlying mechanism of the migraine aura (Lauritzen, 1994; Haerter et al., 2005; Pietrobon, 2005; Welch, 1998; Flippen and Welch, 1997), the KI mice carrying the human FHM-1 R192Q or S218L mutation exhibit a lower threshold for induction of CSD and an increased velocity of CSD propagation (van den Maagdenberg et al., 2004, 2010; Tottene et al., 2009; Eikermann-Haerter et al., 2009). Studies in KI mice revealed multiple gain-of-function effects. The first indication that the gain-of-function of $Ca_V2.1$ channels produced by FHM-1 mutations could lead to enhanced evoked neurotransmitter release was obtained at the neuromuscular junction (NMJ), where evoked neurotransmission was unaltered at physiological Ca^{2+} ion concentrations but increased at 0.2 mM Ca^{2+} in KI mice (Kaja et al., 2005; van den Maagdenberg et al., 2004, 2010). In cerebellar granule cells and cortical pyramidal cells from R192Q KI mice, the current–voltage relationship curves showed an increased in $Ca_V2.1$ Ca^{2+} currents activated at lower voltages, compared to WT mice. This is consistent with the activation of R192Q $Ca_V2.1$ channels at 8–9 mV more negative voltages than the corresponding WT channels (van den Maagdenberg et al., 2004). Using microcultures and brain slices from FHM-1 mice, Tottene et al. (2009) observed an increased probability of glutamate release at the excitatory synapse formed by the cortical layer 2/3 pyramidal cells (PC) and fast-spiking (FS) interneurons, while neurotransmission from the inhibitory GABAergic FS-PC synapses appeared unaltered, despite being mediated by $Ca_V2.1$ channels (i.e., carrying the FHM-1 mutation). This imbalance of cortical excitation and inhibition was associated with increased susceptibility for CSD in the KI mice, but the underlying mechanism changing synaptic strength in the R192Q mutation is not fully understood. At the calyx of Held, presynaptic KI $Ca_V2.1$ channels activate at more hyperpolarized membrane potentials than WT channels. This hyperpolarized activation led to a larger inward Ca^{2+} influx when Ca^{2+} currents were evoked by long duration action potentials (like pyramidal cells APs), but not when Ca^{2+} currents were elicited by short duration APs (like the calyx of Held or interneurons APs), suggesting that the shape and duration of the AP triggering transmitter release may be one factor controlling the expression of a synaptic gain-of-function in the FHM-1 KI mice (González Inchauspe et al., 2012).

$Ca_V2.1$ channels are expressed in all brain structures that have been implicated in the pathogenesis of migraine, including the cerebral cortex, the trigeminal ganglia, and brainstem nuclei involved in the central control of nociception.

Since dysfunctional nociceptive brainstem nuclei might be involved in the pathogenesis of migraine headache, we decided to analyze the biophysical consequences of R192Q $Ca_V2.1$ channel mutation at a synapse of the auditory system where these ion channels are normally expressed, together with other types of Ca^{2+} channels (Giugovaz-Tropper et al., 2011). We used brainstem slices containing the lateral superior olive (LSO), a nucleus of the superior olivary complex. The LSO integrates excitatory inputs driven by sound arriving at the ipsilateral ear with inhibitory inputs driven by sound arriving at the contralateral ear in order to compute interaural intensity differences (IID) for sound localization at high sound frequencies. Ipsilateral excitatory inputs arise from spherical bushy cells of the anterior ventral cochlear nucleus (aVCN) and contralateral inhibitory inputs from the medial nucleus of the trapezoid body (MNTB). So this nucleus allows comparison of both excitatory and inhibitory neurotransmission. We can therefore use this KI animal to explore differential effects of the R192Q mutation on integration of excitatory inhibitory projections in the same neuron. Performing whole cell patch-clamp recordings, we studied glycinergic inhibitory postsynaptic currents (IPSCs) and glutamatergic excitatory postsynaptic currents (EPSCs) onto LSO neurons, in mice carrying the human R192Q FHM-1 mutation. Our data show increased release probability, accompanied by a diminished vesicle pool size, enhanced short-term depression (STD) and faster recovery at both excitatory and inhibitory synapses. However, the strength of excitatory and inhibitory synapses is differently affected: EPSC are severely depressed whereas IPSCs are consistently larger in R192Q KI mice compared to WT mice. We conclude that a gain-of-function of the $Ca_V2.1$ channels in R192Q KI mice, differently affects excitatory and inhibitory synaptic transmission, thereby altering the excitation/inhibition balance.

2. Materials and methods

Generation of the R192Q KI mouse strain was described previously (van den Maagdenberg et al., 2004). In short, codon 192 in exon 4 of the mouse *Cacna1a* gene was modified by gene targeting and now encodes a glutamine instead of an arginine residue. Homozygous R192Q KI and WT mice from the same genetic mixed background of 129 and C57BL/6J were used for our experiments. All experiments were carried out according to National guidelines and approved by local Ethical Committees.

2.1. Preparation of brainstem slices

In this study we used mice of 13–16 days old. This age period was reported to be posterior to maturation of MNTB-LSO synapses, implicating a shift from the co-release of GABA and glycine (Korada and Schwartz, 1999; Kotak et al., 1998; Nabekura et al., 2004), and even release of glutamate (Gillespie et al., 2005) from MNTB terminals onto LSO principal cells, to a predominantly glycinergic MNTB-LSO inhibitory synapse. At the same time, excitatory inputs onto the LSO develop toward an almost exclusively glutamatergic release. In addition, Walcher et al. (2011) showed no developmental changes observed in evoked single-fiber inhibitory amplitudes, or in the number of fibers recruited after hearing onset (P10). Finally, few significant changes in the abundance levels of synaptic proteins were found when R192Q KI mice were compared to WT (Klychnikov et al., 2010).

Mice were killed by decapitation, the brain removed rapidly and placed into an ice-cold low-sodium artificial cerebrospinal fluid (aCSF). The brainstem was mounted in the Peltier chamber of an Integraslice 7550PSDS (Campden Instruments Limited, UK) vibrating microslicer. Transverse slices of 250 μm thickness were cut sequentially and transferred to an incubation chamber containing normal aCSF at 37 °C for 1 h. After incubation the chamber was allowed to return to room temperature. Normal aCSF contained (mM): NaCl 125, KCl 2.5, $NaHCO_3$ 26, NaH_2PO_4 1.25, glucose 10, ascorbic acid 0.5, myo-inositol 3, sodium pyruvate 2, $MgCl_2$ 1 and $CaCl_2$ 2. Low sodium aCSF was as above, but NaCl was replaced by 250 mM sucrose and $MgCl_2$ and $CaCl_2$ concentrations were 2.9 mM and 0.1 mM respectively. The pH was 7.3 when gassed with 95% O_2–5% CO_2.

2.2. Electrophysiology recordings

One slice was transferred to an experimental chamber perfused with normal aCSF at a rate of 1 ml/min. Neurons were visualized using Nomarski optics on a BX50WI (Olympus, Japan) microscope, and a 40X/0.90 NA water immersion objective lens (LUMPlane FI, Olympus). Whole-cell voltage clamp recordings were made with patch pipettes pulled from thin walled borosilicate glass (Harvard Apparatus, GC150F-15, UK). Electrodes had resistances of 2.9–3.2 MΩ when filled with internal solution of the following composition (mM): CsCl 110, Hepes 20, TEA-Cl 10, Na_2phosphocreatine 12, EGTA 0.5, MgATP 2, LiGTP 0.5 and $MgCl_2$ 1; and pH was adjusted to 7.3 with CsOH. To block Na^+ currents and avoid postsynaptic action potentials, 10 mM *N*-(2,6-diethylphenylcarbamoylmethyl)-triethyl-ammonium chloride (QX-314) was added to the pipette solution. Patch-clamp recordings were made using Multiclamp 700B amplifier (Axon CNS, Molecular Devices), a Digidata 1440A (Axon CNS, Molecular Devices) and pClamp 9.0 software. Data were sampled at 50 kHz and filtered at 6 kHz (Low pass Bessel). Whole-cell membrane capacitances (15–25 pF) and series resistances (6–15 MΩ) were measured and quantified from the amplifier and electronically compensated by a 50–60% (Bandwidth > 4 KHz).

Principal neurons were selected from the medial and middle limbs of the LSO, identified by their location and the bipolar and fusiform shape of their soma. Capacitance measurements were employed for the distinction between efferent neurons of the lateral olivocochlear (LOC) and principal neurons. Principal neurons had large size with capacitances larger than 15 pF (Giugovaz-Tropper et al., 2011), in opposition to LOC neurons which have been described to have capacitance values around 6 pF (Sterenborg et al., 2010).

Experiments were conducted under voltage-clamp using whole cell patch recordings at 25 °C.

To evoke IPSCs a bipolar platinum stimulating electrode was located midway between the LSO and the MNTB, and square pulses of 0.1 ms duration and variable voltage amplitudes were applied through an isolated stimulator (Model DS2A, Digitimer Ltd., UK). To isolate glycinergic IPSCs, CNQX (10 μM), DLAP5 (50 μM) and bicuculline (10 μM) were added to the external solution to block glutamatergic AMPA and NMDA and gabaergic mediated synaptic responses respectively. Glutamatergic EPSCs were evoked by positioning the electrode over the ipsilateral fibers from the cochlear nucleus and isolated using strychnine (1 μM), AP5 (50 μM) and bicuculline in the external solution. Miniature inhibitory and excitatory postsynaptic currents (mI/EPSCs) were recorded in the presence of extracellular tetrodotoxin (TTX, 1 μM, from Alomone, Israel).

Calcium channel blockers ω-conotoxin GVIA and ω-agatoxin IVA were purchased from Alomone (Israel) and stocks solutions (10^3 times) were dissolved in pure water and conserved at −20 °C. Stocks solutions (10^3 times) of strychnine were dissolved in DMSO and added to the aCSF at the moment of the experiments.

Data analysis was done using Clampfit 10.0 (Molecular Devices, USA), Sigma Plot 10.0, SigmaStat 3.5 and Excel 2003 (Microsoft) software. Average data are expressed and plotted as mean ± sem. Statistical significance was determined using Student's *t*-test or one way repeated measure ANOVA plus Student-Newman-Keuls post-hoc test. I/EPSC amplitudes (A) as a function of stimulus intensity (Is) for each individual cell plotted in Fig. 2B and D were fitted by a sigmoidal function of the form $A = A_{max}/(1 + \exp((Is\text{-}Is_{1/2})/k))$, where A_{max} is I/EPSCs steady state maximal amplitude and $Is_{1/2}$ is the stimulus intensity for I/EPSC half amplitude. Student's *t*-test was used to compare parameters A_{max} and $Is_{1/2}$ of individual cells for WT and R192Q KI mice. In addition, the fit on the overall data is shown in Fig. 2B and D, which gives nearly the same A_{max} and $Is_{1/2}$ values as the average parameters from individual cell fittings.

3. Results

3.1. Neurotransmitters released (EPSCs/IPSCs) at the LSO

We first confirmed the receptors mediating synaptic transmission at inhibitory MNTB-LSO projections and at excitatory aVCN-LSO projections in P13-P16 WT and R192Q KI mice. Synaptic inputs to the LSO were evoked *in vitro* by electrical stimulation of the presynaptic axons from MTNB and aVCN neurons, respectively. Inhibitory transmission was blocked by strychnine, showing a major contribution by glycine receptors at the MNTB-LSO synapses of both WT and R192Q mice, and in accordance with previous reports (Moore and Caspary, 1983; Sterenborg et al., 2010; Giugovaz-Tropper et al., 2011). Fig. 1A and B shows representative IPSCs in LSO neurons from WT and R192Q KI mice in control conditions and after perfusion of strychnine (2 μM) to block glycine receptors (1A) or (-)-bicuculline methochloride (10 μM) plus 6-ciano-7-nitroquinoxalina-2,3-diona (CNQX; 10 μM) and AP5 (50 μM) to block $GABA_A$, AMPA and NMDA receptors, respectively (1B). A

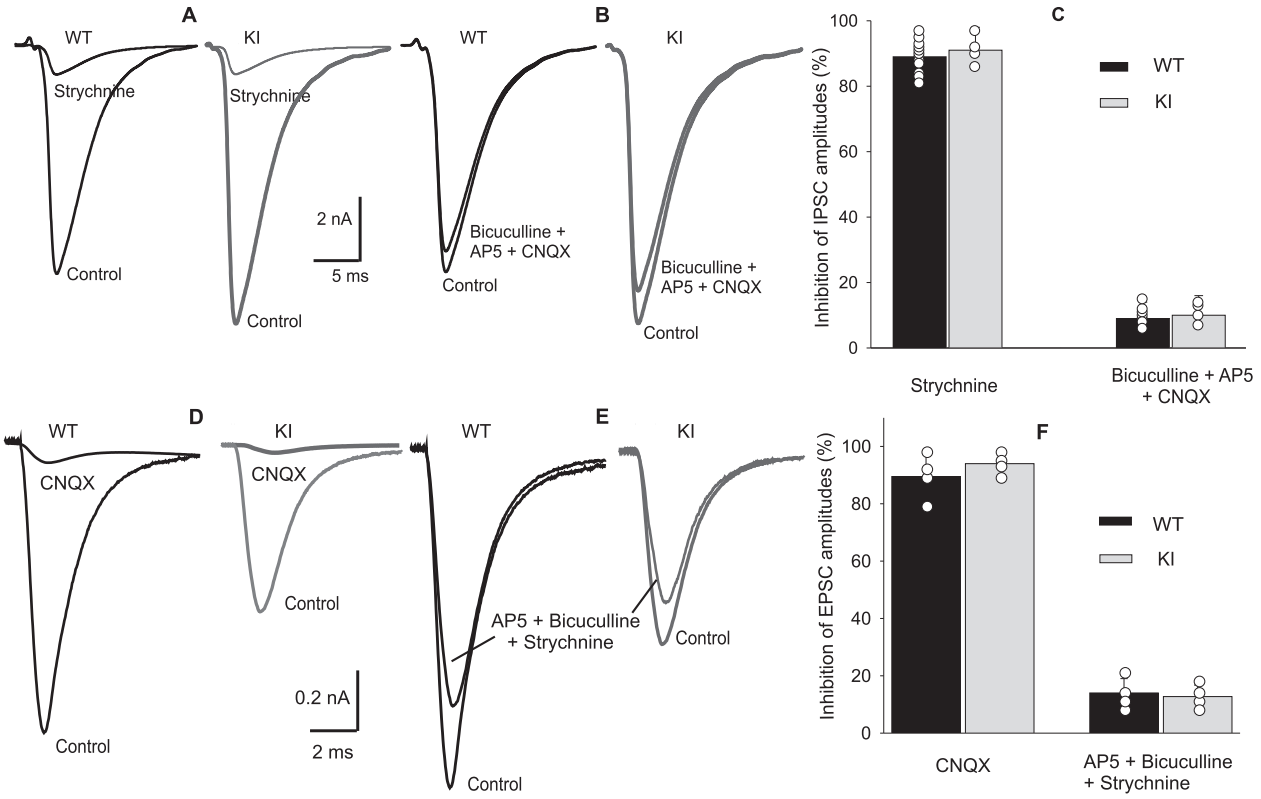

Fig. 1. Contribution of different types of receptor to inhibitory and excitatory synaptic transmission at the LSO in WT and R192Q KI mice. **A**–**B**. Representative IPSCs recorded from neurons of the LSO in WT and R192Q KI mice, under voltage-clamp conditions at a holding potential of −70 mV. IPSCs were evoked by stimulating the innervating axons coming from the MNTB neurons. The contribution from glycine receptors (A) was determined by adding the specific receptor antagonist strychnine (2 μM), while the contribution of $GABA_A$, AMPA and NMDA receptors (B) was assessed by adding (−)-bicuculline methochloride (10 μM) plus 6-ciano-7-nitroquinoxalina-2,3-diona (CNQX; 10 μM) and AP5 (50 μM). **C-** Bars plot summarizing the mean inhibition of IPSCs by strychnine (89 ± 6%, $n = 19$ for WT and 91 ± 7%, $n = 4$ for KI) and by the addition of (−)-bicuculine methochloride together with CNQX and AP5 (9 ± 5%, $n = 24$ for WT and 10 ± 6%, $n = 4$ for R192Q KI mice). **D**–**E**. Representative EPSCs recorded from neurons of the LSO in WT and R192Q KI mice, evoked by stimulating the innervating axons coming from the aVCN. The contribution from AMPA receptors was determined by adding the specific receptor antagonist CNQX 10 μM (D) while the contribution of $GABA_A$, glycine and NMDA receptors was assessed by adding (−)-bicuculline methochloride plus strychnine (2 μM) and AP5 (50 μM). **F**. Bars plot summarizing the mean inhibition of EPSCs by CNQX (89 ± 8%, $n = 4$ for WT and 94 ± 4%, $n = 4$ for R192Q KI) and by the addition of (−)-bicuculine methochloride together with strychnine and AP5 (14 ± 5%, $n = 4$ for WT and 12 ± 4%, $n = 4$ for R192Q KI mice).

summary of receptors contributing to inhibitory synaptic transmission onto LSO neurons from WT and R192Q mice (stimulating afferents from MNTB nucleus) is presented in Fig. 1C. Excitatory transmission was mediated principally by glutamatergic AMPA receptors at the aVCN-LSO synapses of both WT and R192Q KI mice. Fig. 1D and E show representative recordings of EPSC in LSO neurons from a WT and R192Q KI mice in control conditions and after adding CNQX (10 μM) to block AMPA receptors (Fig. 1D) or (−)-bicuculline methochloride (10 μM) plus strychnine (1 μM) and AP5 (50 μM) to block $GABA_A$, glycine and NMDA receptors, respectively (Fig. 1E). Mean contribution of the different types of receptors to excitatory synaptic transmission onto LSO neurons from WT and R192Q KI mice (when stimulating afferents from aVCN nucleus) is presented in Fig. 1F.

We conclude that in mice (P13-16) inhibitory neurotransmission is mainly glycinergic while excitatory synaptic transmission is essentially glutamatergic mediated by AMPA receptors. The R192Q mutation seems not to alter the relative receptor contribution of inhibitory or excitatory LSO afferents, since the pharmacological effects of strychnine and CNQX are similar in the R192Q KI and the WT mice.

The subsequent experiments were made pharmacologically isolating glycinergic IPSCs or glutamatergic AMPA EPSCs to examine the role of FHM-1 R192Q mutation on $Ca_V2.1$ channels in neurotransmitter release at LSO synapses.

3.2. R192Q KI showed lower glutamatergic/glycinergic synaptic ratio compared to WT mice

Neurons in the LSO are innervated by multiple inhibitory and excitatory projections from the MNTB and aVCN, respectively. The evoked synaptic currents will therefore depend on the intensity of the electrical stimuli applied to the innervating axons. Inputs to LSO neurons were stimulated over a range of intensities. Fig. 2A shows representative IPSCs recorded in LSO neurons from WT and R192Q KI mice (holding potential of −70 mV; in the presence of CNQX, (−)-bicuculline and AP5) during increments in the stimulation voltage. IPSC amplitudes from R192Q KI mice ($n = 15$) were significantly larger compared to WT ($n = 19$) for all stimulating intensities above 1.5 V (Figs. 2B, $P < 0.01$, One-way ANOVA RM, Student-Newman-Keuls post-hoc). Mean IPSC maximal amplitudes (measured at steady state, 6 V) were 6.4 ± 0.2 nA in WT mice ($n = 8$) and 8.0 ± 0.3 nA in R192Q KI mice ($n = 9$, $P = 0.001$, Student's t-test). In contrast, EPSC maximal amplitudes (recorded in the presence of strychnine, (−)-bicuculline and AP5) were significantly smaller in R192Q KI compared to WT mice for each stimulus intensity values above 8 V (Fig. 2C). EPSC amplitudes as a function of stimulus are shown in Fig. 2D for WT and KI cells (One-way ANOVA, Student-Newman-Keuls post-hoc, $P < 0.01$). Mean EPSC maximal amplitudes measured at steady state (12 V), were 1.39 ± 0.08 nA in WT ($n = 10$) and 0.69 ± 0.07 nA in R192Q KI mice ($n = 8$, $P = 0.001$,

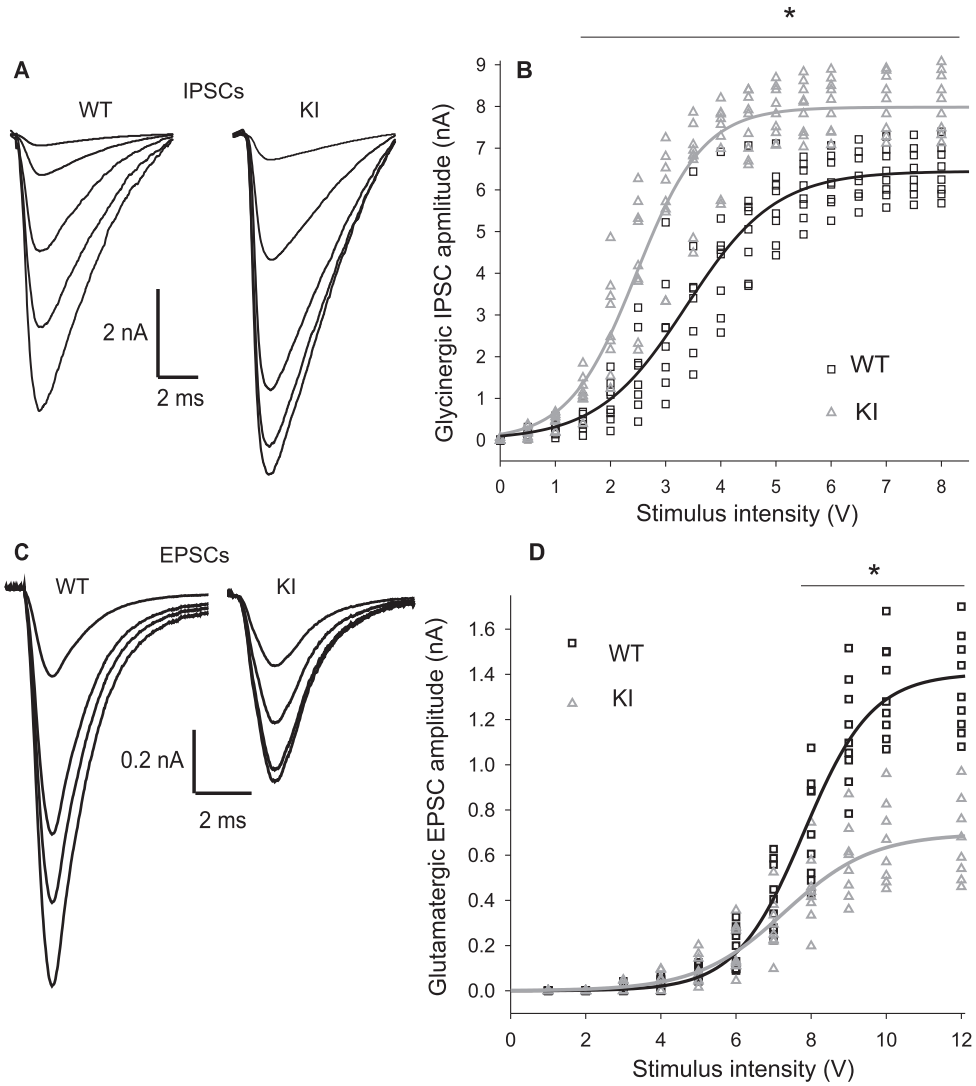

Fig. 2. Evoked release is increased at the inhibitory but decreased at the excitatory LSO synapse. **A**. Representative glycinergic IPSCs recorded from the soma of an LSO neuron under voltage-clamp conditions at a holding potential of −70 mV for different values of the voltage applied to stimulate the innervating axons coming from the MNTB neurons: 1, 2, 4 and 6 V in increasing order for both WT and R192Q KI mice. Traces are the average of 20 stimuli for each stimulating voltage amplitude. **B**. Glycinergic IPSC amplitudes as a function of the voltage amplitude (0.5–8 V) applied to the bipolar platinum stimulating electrode (stimuli of 0.1 ms duration) for WT (black squares, $n = 8$) and R192Q KI (grey triangles, $n = 9$). For each given stimuli intensity above 1.5 V, IPSC amplitudes are larger in R192Q KI mice than in WT mice (*$P < 0.01$, One-way ANOVA RM, Student-Newman-Keuls post-hoc). Data of individual cells were fitted by a sigmoidal function. IPSC maximal amplitudes at steady state (above 6 V) were significantly larger in R192Q KI (mean: 8.0 ± 0.3 nA) than in WT mice (mean 6.4 ± 0.2 nA, $P = 0.001$, Student's *t*-test). The average stimulus intensity for half amplitudes of IPSCs was 3.3 ± 0.6 V ($n = 8$) and 2.5 ± 0.4 V ($n = 9$) for WT and R192Q KI mice respectively ($P = 0.01$, Student's *t*-test). The solid line is the fit of data from all cells together. **C**. Representative glutamatergic EPSCs recorded from the soma of an LSO for different voltage amplitudes applied to the bipolar platinum stimulating electrode: 7, 8, 9 and 10 V in increasing order for both WT and R192Q KI mice. Traces are the average of 20 stimuli for each stimulating voltage amplitude. **D**. Glutamatergic EPSC amplitudes as a function of the voltage amplitude (1–12 V) applied to the bipolar platinum stimulating electrode (stimuli of 0.1 ms duration) for WT (black squares, $n = 10$) and R192Q KI (grey triangles, $n = 8$). For stimuli intensities above 8 V EPSC amplitudes are smaller in R192Q KI mice compared to WT (*$P < 0.01$, One-way ANOVA RM, Student-Newman-Keuls post-hoc). Fitting data for individual cells with a sigmoidal function gives an average parameter for EPSC half amplitude stimulus intensity of 7.8 ± 0.2 V for WT ($n = 10$) and 7.3 ± 0.3 V for R192Q KI mice ($n = 8$, $P = 0.1$, Student's *t*-test). EPSC maximal amplitudes at steady state (above 10 V) were significantly lower in R192Q KI (0.69 ± 0.07 nA) than in WT mice (1.39 ± 0.08 nA, $P = 0.001$, Student's *t*-test). The fit of data from all cells together is also shown.

Student's *t*-test). The kinetics of glycinergic IPSCs and glutamatergic EPSCs from R192Q KI were not statistically different than those from WT mice. IPSCs from WT ($n = 17$) and R192Q KI ($n = 14$) synapses had respectively a mean rise time of 0.37 ± 0.03 ms and 0.32 ± 0.04 ms, mean half width of 2.8 ± 0.2 ms and 2.6 ± 0.3 ms and mean decay time of 6.0 ± 0.6 ms and 5.9 ± 0.7 ms ($P > 0.05$, Student's *t*-test). For EPSCs, mean rise time were 0.72 ± 0.09 ms and 0.78 ± 0.09 ms, mean half width are 1.56 ± 0.34 ms and 1.59 ± 0.18 ms and mean decay time were 2.6 ± 0.7 ms and 2.9 ± 0.6 ms for WT ($n = 9$) and R192Q KI ($n = 8$) mice, respectively ($P > 0.05$, Student's *t*-test).

We next evaluated the probability of vesicle release by estimating the fraction of the ready releasable pool released by a single action potential. We used an approach based on repetitive stimulation mediated short-term depression (STD) of I/EPSC amplitudes. Assuming that depression is largely caused by a transient decrease in the number of readily releasable quanta, it is possible to estimate the pool size by calculating the cumulative summation of integrated I/EPSCs for time intervals that are short with respect to the time required for recovery from depression (Schneggenburger et al., 1999). We considered integrated currents (charge, in pC = nA.ms) instead of current amplitudes in order to take into

account the differences in kinetics between evoked and spontaneous events (in particular for EPSCs) in the subsequent evaluation of the vesicle pool size. We calculated the cumulative sum of integrated I/EPSCs during a train of 20 stimuli at 20 Hz in WT and R192Q KI mice. Data points in the range between 0.55 s and 1.0 s were fitted by linear regression and back-extrapolated to time 0 (Fig. 3A for IPSCs and Fig. 3C for EPSCs). This estimation effectively takes into account the cumulative integrated I/EPSCs reached within the first six stimuli, corresponding to a time interval of about 0.25 s, before depression reaches its steady state level. It assumes that recovery from depression is negligible for the time interval of about 0.25 s used for the calculation. The validity of this assumption can be assessed in the analysis of time recovery from STD described below (See section 2.4 and Figs. 5C and F). The zero time intersect gives an estimate of the size of the readily releasable pool of synaptic vesicles (N) multiplied by the mean quantal integrated current (q). The release probability can be estimated by dividing the mean integrated current of the first evoked I/EPSC in the train by the Nq

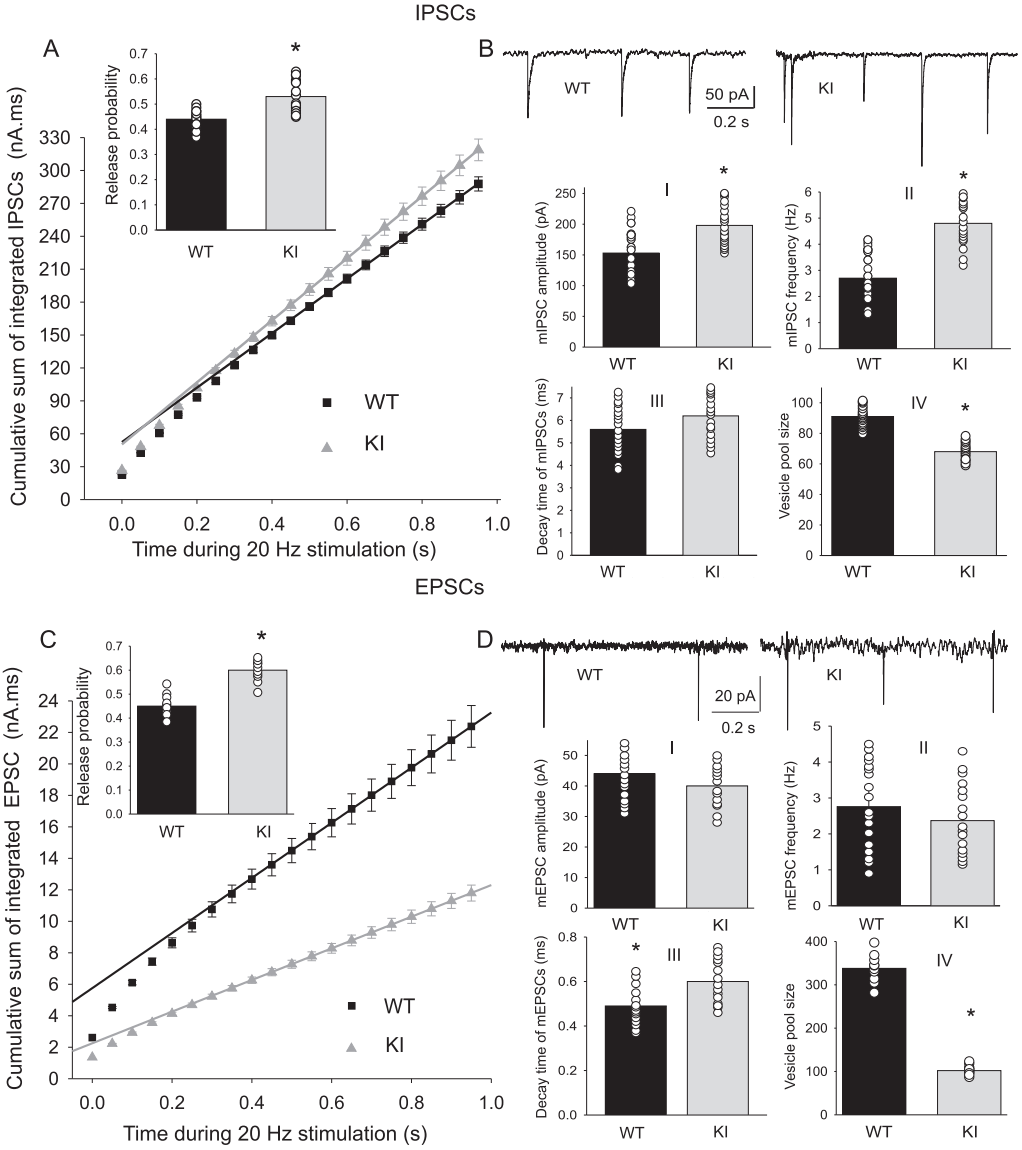

Fig. 3. R192Q KI mice present a higher release probability **A**. Mean cumulative summation of integrated IPSCs during 20 Hz stimulation in WT and R192Q KI mice as a function of time. A lineal function was fitted to the steady state region for times larger than 0.55 s and back-extrapolated to time 0, to estimate the readily releasable pool size (N) multiplied by the mean quantal integrated current (q). The Nq values obtained for WT and KI are 52.4 ± 1.4 nA ms and 50 ± 1 nA ms respectively. ***Inset***: The release probability (calculated as the ratio between the mean integrated current of the first IPSC in the train and the Nq value) is significantly higher in R192Q KI (0.53 ± 0.02, $n = 15$) than in WT synapses (0.44 ± 0.01, $n = 15$; $P = 2.10^{-5}$, Student's t-test). **B**. Spontaneous inhibitory release. Mean amplitudes (**I**) of mIPSC are increased in R192Q KI mice (198 ± 13 pA, $n = 19$) compared to WT (153 ± 7 pA, $n = 30$, $P = 0.002$ Student's t-test) and so are the frequencies (**II**): 4.8 ± 0.4 Hz in R192Q KI vs 2.7 ± 0.2 Hz in WT mice ($P = 10^{-5}$, Student's t-test). Decay time constants of mIPSCs (**III**) present no statistical differences between KI (6.2 ± 0.7 ms) and WT mice (5.6 ± 0.5 ms, $P = 0.07$, Student's t-test). The estimated vesicle pool size (**IV**) is diminished at inhibitory synaptic transmission from R192Q KI (68 ± 6, $n = 15$) compared to WT (91 ± 7, $n = 15$, $P = 0.01$, Student's t-test). **C**. Mean cumulative summation of integrated EPSCs during 20 Hz stimulation in WT and R192Q KI mice as a function of time. The Nq values obtained for WT ($n = 10$) and KI ($n = 11$) are 5.7 ± 0.4 nA ms and 2.3 ± 0.1 nA ms, respectively. ***Inset***: The release probability is significantly higher in KI (0.60 ± 0.03, $n = 11$) than in WT synapses (0.45 ± 0.02, $n = 10$; $P = 4\ 10^{-6}$, Student's t-test). **D**. Spontaneous excitatory release. Mean amplitudes (I) of mEPSC are similar in R192Q KI mice (40 ± 3 pA, $n = 17$) compared to WT (44 ± 5 pA, $n = 19$, $P > 0.05$, Student's t-test) and so are the frequencies (II): 2.4 ± 0.4 Hz in KI and 2.7 ± 0.4 Hz in WT, $P > 0.05$, Student's t-test. Decay time constants of mEPSCs (III) are higher in KI (0.60 ± 0.04 ms) compared to WT mice (0.49 ± 0.04 ms, $P = 0.02$, Student's t-test). Mean vesicle pool size is diminished at excitatory synaptic transmission from R192Q KI (104 ± 13, $n = 11$) compared to WT (335 ± 30, $n = 10$, $P = 10^{-6}$, Student's t-test).

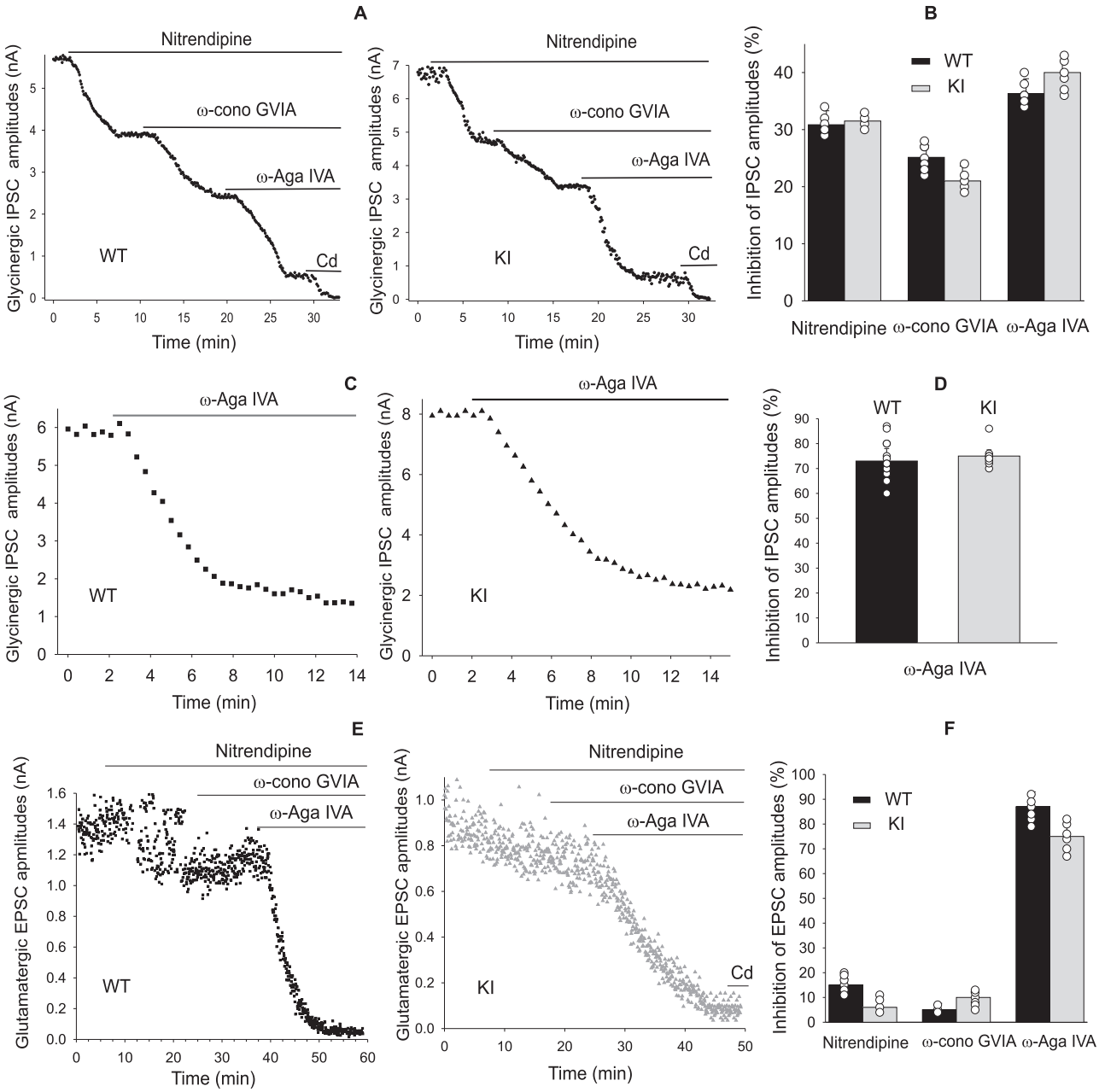

Fig. 4. Ca^{2+} channel involved in inhibitory and excitatory synaptic transmission at the LSO from WT and R192Q KI mice. **A**. Peak amplitudes of glycinergic IPSCs recorded at a holding potential of −70 mV as a function of time during the sequential application of selective L-, N- and P/Q-type Ca^{2+} channel antagonists: nitrendipine (10 μM), ω-conotoxin-GVIA (2 μM) and ω-agatoxin IVA (200 nM), respectively, in WT (left) and KI mice (right). Horizontal bars indicate the time of drug application. **B**. Average contribution of each channel type to the total glycinergic IPSCs determined by subtracting current amplitudes before and after application of the specific blockers as state in A. The L-type component is 30.8 ± 0.8% and 31.5 ± 0.8% in WT ($n = 7$) and KI ($n = 6$) mice respectively ($P = 0.45$, Student's t-test). The P/Q-type component is 36 ± 1% ($n = 7$) in WT and 40 ± 2% ($n = 6$) in KI ($P = 0.05$, Student's t-test). The N-type component is 25 ± 2% in WT ($n = 7$) and 21 ± 2% in KI ($n = 6$, $P = 0.06$, Student's t-test). **C-** Effect of ω-agatoxin IVA (200 nM) on IPSC amplitudes when this channel blocker is applied alone in WT and KI LSO synapses. **D-** Mean IPSC amplitude inhibition when only P/Q-type Ca^{2+} channels are blocked: 73 ± 5% in WT ($n = 5$) and 75 ± 3% in KI ($n = 9$). **E**. Peak amplitudes of glutamatergic EPSCs as a function of time during the sequential application of L-, N- and P/Q-type Ca^{2+} channel antagonists in WT (left) and R192Q KI mice (right). Horizontal bars indicate the time of drug application. **F**. Average contribution of each channel type to the total glutamatergic EPSCs. Excitatory transmission is predominantly mediated by P/Q-type Ca^{2+} channels: 87 ± 6% ($n = 7$) in WT and 75 ± 5% ($n = 6$) in KI ($P = 0.05$, Student's t-test). The L-type Ca^{2+} channels contribute with 15 ± 3% in WT ($n = 7$) and 6 ± 5% in KI mice ($n = 6$, $P = 0.36$, Student's t-test) while the N-type Ca^{2+} channels contribute with 5 ± 2% en WT ($n = 7$) and 10 ± 2% in KI ($n = 6$, $P = 0.4$, Student's t-test).

value. Although this calculation may be overestimated because Ca^{2+} influx during the first stimulus is lower than during the last pulses and Ca^{2+} concentration rises during stimulation, the comparison between genotypes indicated that the release probability was significantly higher in R192Q KI than in WT mice at both inhibitory (Fig. 3A inset, $P = 2.10^{-5}$, Student's t-test) and excitatory (Fig. 3C inset, $P = 4.10^{-6}$, Student's t-test) synapses onto LSO neurons.

An estimate of the quantal integrated current can be obtained from the integrated currents of spontaneous miniature events (mI/EPSCs). The amplitude of the mIPSCs measured in R192Q KI mice (198 ± 13 pA, $n = 19$) were larger than mIPSC amplitude measured

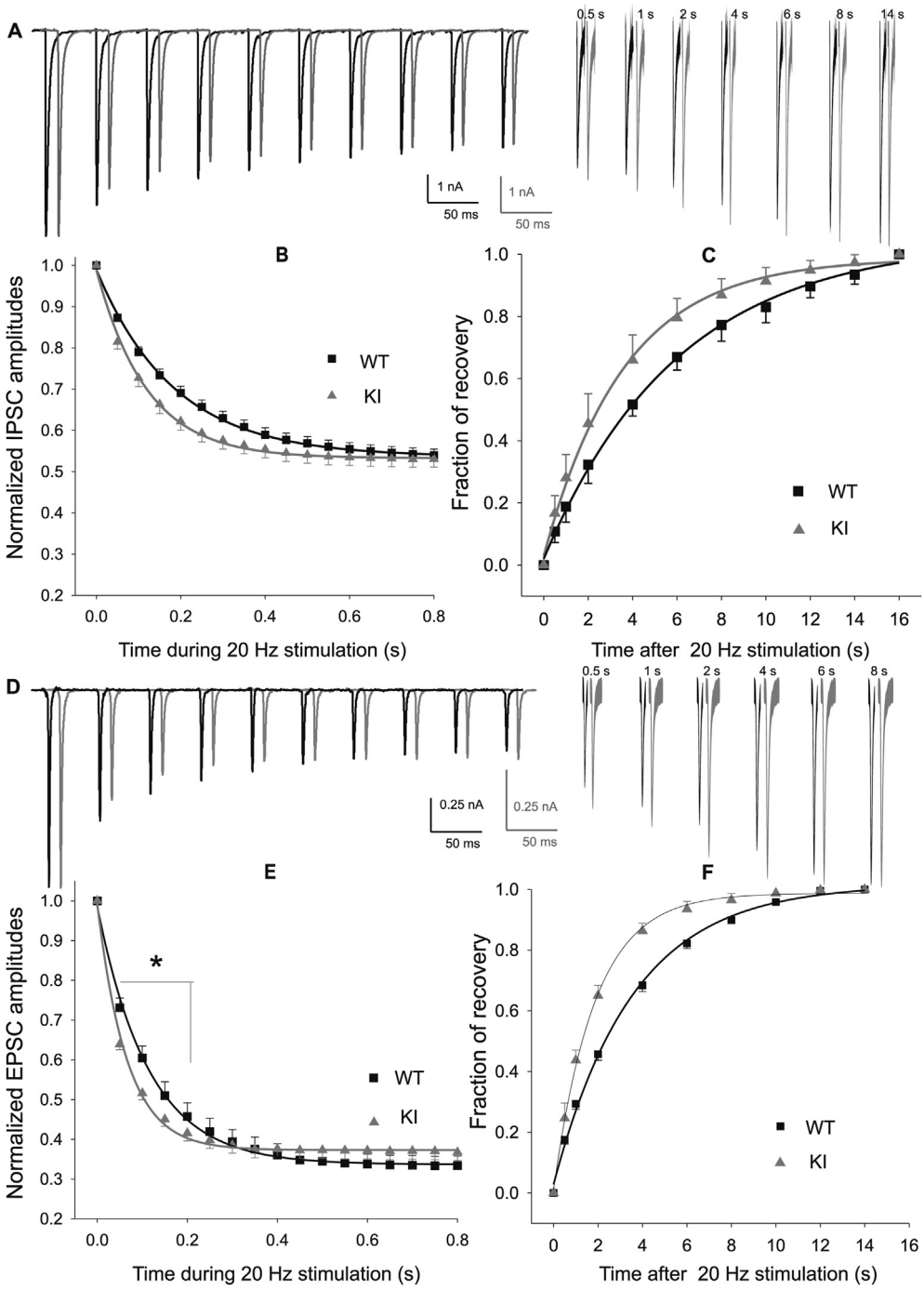

Fig. 5. Enhanced short-term plasticity at inhibitory and excitatory synaptic transmission in R192Q KI compared to WT mice. **A**. Traces showing depression of IPSC amplitudes during stimulation at 20 Hz (conditioning train) and recovery at different time delays after the conditioning train (WT: black traces; R192Q KI: grey traces shifted to the left, note the different amplitude scales for WT and KI). Stimulation artefacts have been deleted for clarity. **B**. Time course of depression of IPSC amplitudes during 1 s stimulation at 20 Hz (conditioning train, recorded at a holding potential of −70 mV). The amplitudes are normalized to the first IPSC amplitude in the train. Data are fitted to a single exponential decay function, with a decay time constant $\tau = 0.183 \pm 0.013$ s in WT ($n = 15$) and $\tau = 0.120 \pm 0.020$ s in KI R192Q ($n = 15$, $P = 10^{-4}$, Student's *t*-test). The depressed IPSC amplitudes at the end of the stimuli reached a steady state value of 54 ± 2% and 53 ± 2% of the first IPSC amplitude in the train, in WT and KI R192Q synapses respectively ($P = 0.055$, Student's *t*-test). C. Time course of recovery from synaptic depression, measured by eliciting a single test IPSC at increasing time intervals following the 20 Hz conditioning train. The fraction of recovery is calculated as $(I_{test} - I_{ss})/(I_1 - I_{ss})$, where I_1 and I_{ss} are the amplitudes of the first and last IPSCs in the train and I_{test} is the amplitude of the test IPSC. Data are fitted to an exponential decay function of first order, with time constants $\tau = 6.0 \pm 0.2$ s ($n = 15$) and $\tau = 3.6 \pm 0.2$ s ($n = 15$) for WT and R192Q KI respectively ($P = 10^{-4}$, Student's *t*-test). **D**. Traces showing depression of EPSC amplitudes during stimulation at 20 Hz (conditioning train) and recovery at different time delays after the conditioning train (WT: black traces; R192Q KI: grey traces shifted to the left, note the different amplitude scales for WT and KI). Stimulation artefacts have been deleted for clarity. **E**. Time course of depression of EPSC amplitudes, normalized to the first EPSC of the 20 Hz train. Amplitudes of the EPSCs at the end of the stimuli are 34 ± 3% and 37 ± 3% of the first pulse for WT ($n = 10$) and R192Q KI ($n = 11$, $P > 0.05$, Student's *t*-test), respectively. Data are fitted with a single exponential decay function, with a time constant $\tau = 0.114 \pm 0.012$ s en WT ($n = 10$) and $\tau = 0.066 \pm 0.004$ s en KI R192Q ($n = 11$, $P = 0.003$, Student's *t*-test). F. Recovery of EPSCs after a 1 s train at 20 Hz follows an exponential time course with time constants $\tau = 3.5 \pm 0.3$ s ($n = 10$) and $\tau = 1.86 \pm 0.12$ s ($n = 11$) for WT and R192Q KI respectively ($P = 10^{-5}$, Student's *t*-test).

in WT mice (153 ± 7 pA, $n = 30$, $P = 0.002$, Figs. 3B, I); mIPSC frequencies were also higher in synapses from R192Q KI (4.8 ± 0.4 Hz, $n = 16$) compared to synapses from WT mice (2.7 ± 0.2 Hz, $n = 32$, $P = 10^{-5}$, Student's *t*-test, Fig. 3B, II). Decay times of mIPSCs were not statistically different between R192Q KI (6.2 ± 0.7 ms) and WT mice (5.6 ± 0.5 ms, $P = 0.07$, Student's *t*-test, Fig. 3B, III). Mean integrated currents of mIPSCs were 740 ± 50 pA ms and 575 ± 26 pA ms, for R192Q KI and WT mice respectively ($P = 0.001$, Student's *t*-test). The estimated vesicle pool size was obtained dividing the zero time intersect of the cumulative IPSC amplitudes by the quantal integrated current q. This value was slightly smaller in R192Q KI (68 ± 6, $n = 15$) compared to WT mice (91 ± 7, $n = 15$), $P = 0.008$, Student's *t*-test, Fig. 3B, IV).

Different results were found for the excitatory transmission. Miniature EPSC measured from R192Q KI and WT mice had similar amplitudes (40 ± 3 pA, $n = 17$ in KI and 44 ± 5 pA, $n = 19$ in WT, $P > 0.05$, Student's *t*-test, Figs. 3D, I) and similar frequencies (2.4 ± 0.4 Hz in KI and 2.7 ± 0.4 Hz in WT, $P > 0.05$, Student's *t*-test, Fig. 3D, II). Interestingly mEPSC decay times were larger in KI (0.60 ± 0.04 ms) compared to WT (0.49 ± 0.04 ms, $P = 0.02$, Student's *t*-test, Fig. 3D, III). Mean integrated currents of mEPSCs were larger in R192Q KI (22 ± 2 pA ms) than in WT mice (17 ± 2 pA ms, $P = 0.005$, Student's *t*-test).

The ready releasable pool size was severely reduced in R192Q KI (104 ± 13, $n = 11$) compared to WT mice (335 ± 30, $n = 10$, $P = 10^{-6}$, Student's *t*-test, Fig. 3D, IV).

We conclude that FHM-1 R192Q mutation increased release probability and decreased pool size at both synapses (aiming to a presynaptic effect), even though the IPSC conductance was larger and the EPSC conductance was smaller in R192Q KI compared to WT mice.

3.3. Ca^{2+} channels involved in inhibitory and excitatory synaptic transmission in WT and R192Q KI mice

The subtypes of Ca^{2+} channels mediating synaptic transmission were assessed by using specific blockers of the calcium channels. I/EPSCs, evoked at a holding potential of −70 mV, were recorded during sequentially bath application of nitrendipine (10 μM, L-type antagonist), ω-conotoxin GVIA (2 μM; N-type blocker), ω-agatoxin IVA (0.2 μM; P/Q-type blocker) and cadmium (50 μM; non-selective Ca^{2+} channel blocker). Representative plots of I/EPSC peak amplitudes as a function of time are shown in Fig. 4A (IPSCs) and Fig. 4E (EPSCs) for both WT and R192Q KI mice. The relative contribution of each type of Ca^{2+} channel to the evoked synaptic currents was determined from the fraction of IPSC amplitudes inhibited by the application of the selective Ca^{2+} channel antagonist applied in the sequence shown in Figs. 4A and E.

IPSCs were triggered by multiple types of VACC (Figs. 4B, $n = 7$ for WT and $n = 6$ for R192Q KI mice), with no significant differences between the two genotypes. In synapses where multiple VACCs are involved in triggering transmitter release, the degree of cooperativity and efficiency of each type of Ca^{2+} channel depends on their distribution at different release sites and on the distance between the channel and the release sites (Neher and Sakaba, 2008; Schneggenburger et al., 2002; Wu et al., 1999). The cooperative action of Ca^{2+} on the calcium sensor is reflected in the dependence of the transmitter release on the third or fourth power of the presynaptic calcium influx (Fedchyshyn and Wang, 2005; Yang and Wang, 2006; Takahashi and Momiyama, 1993; Wu and Saggau, 1997). Hence, the inhibitory effect of Ca^{2+} channel blockers on IPSCs depends on the order in which drugs are applied, indicating that the effect of each toxin does not cause a linear reduction of release. The effect of ω-agatoxin IVA applied alone (representative traces in Fig. 4C) inhibited IPSC by 73 ± 5% ($n = 5$) and 75 ± 3% ($n = 9$) in WT and R192Q KI mice respectively (Fig. 4D).

On the other hand, EPSCs were predominantly mediated by $Ca_V2.1$ Ca^{2+} channels (Figs. 4E, F) in both WT (87 ± 6%, $n = 7$) and R192Q KI mice (75 ± 5%, $n = 6$), with no significant differences between the two genotypes.

These results indicate that $Ca_V2.1$ VACCs play a predominant role at both excitatory and inhibitory LSO synapses.

3.4. Short-term plasticity in synaptic transmission of R192Q KI

Repetitive stimulation of the LSO synapses causes STD of both excitatory and inhibitory transmission. IPSC and EPSC amplitudes decrease during the train of stimuli until they reach a steady state. EPSCs exhibit stronger STD and a faster decay time course than IPSCs (compare Fig. 5A and B with Fig. 5D and E for inhibitory and excitatory transmission respectively).

In order to compare WT and R192Q KI synaptic behaviour, we studied the time-course of STD and recovery after 20 Hz stimulation at the LSO inhibitory (Fig. 5A) and excitatory (Fig. 5D) synapses. At both synapses the amplitude of the synaptic currents measured in KI depressed with a faster time course compared to WT. Nevertheless the magnitude of depression at the end of the stimuli was similar between WT and KI mice. Plot of mean IPSC amplitudes as a function of time during stimulation was fitted to a single exponential decay function, with a decay time constant $\tau = 183 \pm 13$ ms in WT ($n = 15$) and $\tau = 120 \pm 20$ ms in R192Q KI ($n = 15$, $P = 10^{-4}$, Student's *t*-test).

Time course of EPSC amplitudes during 20 Hz STD was fitted with a single exponential decay function, with a time constant $\tau = 114 \pm 12$ ms in WT ($n = 10$) and $\tau = 66 \pm 4$ ms in R192Q KI ($n = 11$, $P = 0.003$, Student's *t*-test).

The time course of recovery from synaptic depression was studied by eliciting a single test I/EPSC at varying time intervals (from 0.1 s to 20 s) following the conditioning train. The fraction of recovery was calculated as follows:

$$\text{Fraction of recovery} = (I_{\text{test}} - I_{\text{ss}})/(I_1 - I_{\text{ss}})$$

where I_1 and I_{ss} are the amplitudes of the first and last I/EPSCs in the train and I_{test} is the amplitude of the test I/EPSC.

The fraction of recovery from STD as a function of time after a 20 Hz stimulus train could be fitted by a single exponential for R192Q KI and WT mice. In line with the stronger STD, excitatory inputs recovered much faster than inhibitory inputs (compare Figs. 5C and F). Plots of mean I/EPSC amplitudes as a function of time delay after the train stimuli, with the corresponding parameters of the exponential fitting are shown in Fig. 5C (inhibitory) and Fig. 5F (excitatory). Comparing the two genotypes, we found that the rate of recovery was significantly increased in R192Q KI compared to WT mice, for both inhibitory and excitatory inputs to the LSO neurons. These results support evidence on the importance of Ca^{2+} influx through $Ca_V2.1$ Ca^{2+} channels in the refilling of the releasable pool of synaptic vesicles: mutations in calcium channels may alter STD and or vesicle replenishment.

4. Discussion and conclusion

4.1. $Ca_V2.1$ Ca^{2+} channels play a central role at excitatory and inhibitory synaptic afferents to LSO

Most of the current evidence points to CSD, the phenomenon that underlies the migraine aura, as the most probable primary cause of activation of the trigeminovascular system and consequent headache. An alternative view considers that migraine aura and

headache are parallel rather than sequential processes. In this sense, CSD can activate the meningeal trigeminovascular afferents and evoke a series of alterations in the meninges and brainstem that modulate trigeminal nociceptive inputs (Akerman et al., 2011; Pietrobon and Striessnig, 2003). Using knock-in mice carrying the pathogenic FHM-1 mutation R192Q in neuronal $Ca_V2.1$ (P/Q-type) Ca^{2+} channels, we evaluated the functional consequences of this mutation on inhibitory and excitatory synaptic transmission at the LSO using brainstem auditory slices. Excitatory glutamatergic release was principally dependent on $Ca_V2.1$ Ca^{2+} channels (Figs. 4E, F). Inhibitory glycinergic release was, on the other hand, mediated by multiple VACCs (Figs. 4A, B). The relative contribution of the different type of Ca^{2+} channels to inhibitory and excitatory synaptic transmission was the same in WT and R192Q KI mice. Therefore, no mechanism for compensation of the gain of function of $Ca_V2.1$ channels was observed. It is important to recall that $Ca_V1.3$ (L-type) Ca^{2+} channels have been demonstrated to be indispensable for the development and refinement of inhibitory synapses in the LSO (Hirtz et al., 2011, 2012). The degree of cooperativity and efficiency of each subtype in controlling transmitter release depends on the distribution of the different subtypes of Ca^{2+} channels at different release sites (Mintz et al., 1995; Reid et al., 1998). Calcium influx through VACCs increases intracellular Ca^{2+} concentration in a bell-shaped microdomain close to the channel mouth (Llinas and Moreno, 1998) which can be modulated by factors that alter calcium buffering and/or diffusion, with a large effect on calcium-triggered cellular events. So, the degree of cooperativity and efficiency of each type of Ca^{2+} channels in controlling transmitter release will also depends on the distance between the channel, the calcium sensor and the release sites (Neher and Sakaba, 2008; Schneggenburger et al., 2002; Wu et al., 1999). The inhibitory effect of Ca^{2+} channel blockers on IPSCs depends on the order in which each drug is applied. The dependence of the transmitter release on the third or fourth power of the presynaptic calcium influx indicates a cooperative action of Ca^{2+} on the calcium sensor (Fedchyshyn and Wang, 2005; Yang and Wang, 2006; Takahashi and Momiyama, 1993; Wu and Saggau, 1997). When the $Ca_V2.1$ blocker ω-agatoxin IVA was applied alone in WT and R192Q KI mice, IPSCs were inhibited by more then 70% (Figs. 4C, D). These data reveal that release of vesicle at both excitatory and inhibitory synaptic transmission strongly depends on calcium influx via $Ca_V2.1$ channels and suggest that $Ca_V2.1$ Ca^{2+} channels are more suitable for triggering transmitter release and have an efficient and dominant role in controlling neurotransmitter release at central excitatory and inhibitory synapses. It is worth mentioning that the participation of $Ca_V2.1$ calcium channels in the inhibitory and excitatory neurotransmission onto LSO synapses is opposite to that in cortical synapses. Excitatory glutamatergic neurotransmission at connected pairs of layer 2/3 pyramidal cells (PC) and multipolar fast-spiking (FS) interneurons in cortical slices of the somatosensory cortex of WT and KI mouse cortical slices was cooperatively mediated by N-, P/Q- and R-type Ca^{2+} channels, while the FS-PC inhibitory synaptic transmission was exclusively triggered by $Ca_V2.1$ calcium channels (Tottene et al., 2009).

The finding that N-type and L-type calcium channels contribute to IPSC release is in agreement with previous studies (Alamilla and Gillespie, 2013). This situation is not unusual within developed CNS synapses. For example N-type calcium channels persistently contribute to cerebral cortical EPSCs and spinal IPSCs throughout postnatal months (Westenbroek et al., 1992, 1998; Iwasaki et al., 2000). Previous studies reported that is a clear developmental trend in the relative contribution of the different voltage gated calcium channels (VGCC) to inhibitory neurotransmission (Alamilla and Gillespie, 2013; Iwasaki and Takahashi, 1998). Changes occur during the first 10 postnatal days, and by the hearing onset the composition of calcium channels controlling neurotransmitter release is stable. We therefore exclude that the changes here observed are linked to development.

4.2. Differential effect of R192Q $Ca_V2.1$ mutation on inhibitory and excitatory synaptic response and release probability

FHM-1 R192Q mutation affected inhibitory and excitatory LSO synapses in a different way. As expected from a multiple innervated neuron, IPSC and EPSC amplitudes were dependent on the number of axons recruited during stimulation. At the inhibitory MNTB-LSO synapse, the FHM-1-mutated $Ca_V2.1$ Ca^{2+} channels resulted in a functional synapse with increased amplitudes of evoked IPSCs in R192Q KI compared to WT mice. In contrast, at the excitatory aVCN-LSO synapse, the mutation gave rise to a reduction in the strength of the EPSC in R192Q KI compared to WT mice. Spontaneous release showed increased amplitudes of mIPSCs while amplitudes of mEPSCs remained unaltered in R192Q KI compared to WT mice. Frequencies of mIPSCs (but not of mEPSCs) were increased in R192Q KI compared to WT mice.

At both inhibitory and excitatory neurotransmission, FHM-1 R192Q mutation resulted in a higher release probability in R192Q KI compared to WT. The increment in release probability suggests a presynaptic effect of the FHM-1 mutation, which produces an increase in AP−evoked calcium influx. The increase in presynaptic activity was previously investigated at the calyx of Held-MNTB synapse, where the big size of the presynaptic terminals allowed electrophysiological patch-clamp recordings of presynaptic Ca^{2+} currents (González Inchauspe et al., 2012). It was reported that R192Q mutated $Ca_V2.1$ channels activated at more hyperpolarizing potentials and that presynaptic Ca^{2+} currents had a faster kinetics of activation. This small shift in voltage dependent activation would lead to an increase in Ca^{2+} influx near the release sites during evoked action potentials in the mutant mice. On the other hand, a reduced size of the readily releasable pool of vesicles was observed at R192Q KI synapses, more prominent in the excitatory synapse (69% of reduction in R192Q KI compared to WT mice) than in the inhibitory synapse (25% of reduction in R192Q KI compared to WT mice).

The enhanced inhibitory neurotransmission is what would be predicted by the change in mIPSC amplitudes and by the increase in release probability occurring in the calyx terminals. These two factors more than compensate the slightly reduced vesicle pool size. Moreover, the change in vesicle pool could indicate the occurrence of a mechanism that preserves synaptic transmission in face of a dramatic augment of inhibition.

The release probability was also increased at the excitatory glutamatergic nerve terminals. However, the severe reduction in vesicle pool size together with the unchanged mESPC amplitudes resulted in an overall reduction of the excitatory synaptic currents here reported, aiming to recover the balance between excitation and inhibition in R192Q KI synapses. These findings suggest the possible occurrence of homeostatic compensatory mechanisms, which could be different at inhibitory or excitatory synapses (Turrigiano, 2012). At this regard, it is important the finding that $Ca_V2.1$ channels are involved in homeostatic modulation of presynaptic neurotransmitter release at the Drosophila neuromuscular junction (Frank et al., 2009).

It is interesting to point out that in contrast to our findings at the LSO synapses, at the somatosensory cortical synapses studied by Tottene et al. (2009) there was an enhancement in excitatory glutamatergic neurotransmission at the PC-FS connection in R192Q KI compared to WT mice while the inhibitory GABAergic neurotransmission at FS-PC connections was unaffected by the FHM-1 R192Q mutation. Interestingly it seems that at these synapse

there were no homeostatic compensatory mechanisms. In summary, in synapse from R192Q KI mice, the balance between excitation and inhibition is lost. The differential effect of FHM-1 mutations on excitatory and inhibitory neurotransmission at different synapses may produce over-excitation in certain conditions, but may leave the excitation-inhibition balance within physiological limits in others.

4.3. R192Q $Ca_V2.1$ mutation enhances short term plasticity

Most relevant was the effect of the FHM-1-mutated $Ca_V2.1$ Ca^{2+} channels on short-term synaptic plasticity. Firstly, it is worth mentioning that excitatory transmission depressed and recovered much faster than inhibitory transmission, independently of the genotypes (compare Fig. 5 B with Fig 5 E for depression and Fig. 5 C with Fig 5 F for recovery). This suggests that the relative EPSC and IPSC amplitudes might dynamically change during periods of prolonged stimulation. Comparing between genotypes, the time course of STD and recovery during 20 Hz frequency stimulation was faster in R192Q KI mice at both excitatory and inhibitory LSO synapses. STD is the consequence of depletion of the release-ready vesicle pool (Wang and Kaczmarek, 1998; Wu and Borst, 1999; Schneggenburger et al., 1999; von Gersdorff and Borst, 2002; Wong et al., 2003; Zucker and Regehr, 2002), although other mechanisms like receptor desensitization (Neher and Sakaba, 2001; Taschenberger et al., 2002; Wong et al., 2003; Schneggenburger et al., 2002), calcium channel inactivation (Forsythe et al., 1998; Xu and Wu, 2005; Muller et al., 2008) and calcium channel inhibition by presynaptic metabotropic glutamate receptor (Von Gersdorff et al., 1997; Takahashi et al., 1996) or AMPA receptors activation (Takago et al., 2005; Scheuss et al., 2002; Neher and Sakaba, 2001) may be involved. The efficacy of synaptic transmission during repetitive stimulation is also determined by the rate of recovery from synaptic depression. Postsynaptic currents recover from STD after many seconds of rest due to recycling of vesicles into the ready releasable pool (Zucker and Regehr, 2002), which is dynamically regulated by Ca^{2+} influx through voltage-gated Ca^{2+} channels in an activity dependent manner which is highly dependent on the recent history of synaptic activity (Wang and Kaczmarek, 1998). High-frequency stimulation of presynaptic terminals significantly enhances the rate of replenishment. Wang and Kaczmarek (1998) have shown that Ca^{2+} influx through voltage-gated Ca^{2+} channels is the key signal that dynamically regulates the refilling of the releasable pool of synaptic vesicles in response to different patterns of inputs. Therefore, mutations in calcium channels may alter STD and or vesicle replenishment. Considering that a substantial amount of synaptic depression is due to vesicle depletion, the enhanced short-term depression (STD) and diminished pair pulse ratio (PPR) in R192Q KI mice (Figs. 5B, E) is consistent with the higher release probability (Figs. 3A, C, insets) and the smaller vesicle pool size (Figs. 3B, D) that these transgenic mice exhibited at both excitatory and inhibitory synapses, reinforcing the hypothesis of a presynaptic effect of the FHM-1 mutation.

The enhanced rate of recovery from STD observed in R192Q KI mice is an important feature that can modify synaptic efficacy and excitability. It suggests a faster recycling rate of vesicles into the ready releasable pool (Wang and Kaczmarek, 1998), and is in agreement with the enhanced preceding synaptic activity (enhanced STD as shown in Figs. 5B, E). Faster recovery in excitatory and inhibitory transmission might be due to an increased residual Ca^{2+} in synapses from R192Q KI mice, responsible for accelerating vesicle endocytosis and refilling process following STD. The rise in residual calcium is a consequence of the mutated $Ca_V2.1$ channels as was described at the calyx of Held synapse (González Inchauspe et al., 2010, 2012). It is worth mentioning that the faster recovery in the R192Q KI model is opposite to the effect observed in knock-out mice with ablated $Ca_V2.1$ channels (α_{1A} −/−). Synapses from α_{1A} −/− mice show a slower kinetics of recovery after STD compared to WT mice (Giugovaz-Tropper et al., 2011; González Inchauspe et al., 2007). Faster recovery of vesicle recycling during repetitive activity may also contribute to the increased excitability in FHM-1 mutant mice. Although further studies are needed to determine the exact mechanism involved in the alteration of short-term plasticity observed in the FHM-1 transgenic migraine mouse model, it is very likely that the increased rate of recovery could result in important changes in network activity and to dysfunction.

Neurons in the LSO are responsible of processing ILD. Precise ILD is achieved by integrating ipsilateral excitatory and contralateral inhibitory inputs which must converge with sub-millisecond precision (Joris and Yin, 1995; Tollin, 2003). The kinetics of glycinergic IPSCs and glutamatergic EPSCs were not affected by the mutation. We would therefore expect the ILD not to be affected. However, we cannot exclude that changes in the amplitudes of the currents and in short term plasticity might affect temporal fidelity along the inhibitory and/or excitatory pathway. It might therefore be interesting to measure ILD sensitivity in KI mice. The different impact of the mutation on excitatory and inhibitory synaptic transmission may prevent proper ILD encoding.

To allow comparison with *in vivo* data, we should however reexamine the impact of the mutation on synaptic inputs recorded at a physiological temperature of 37 °C and we cannot assure that effects here observed on release probability, short term depression and recovery will be affected to the same degree.

5. Conclusions

The demonstration that FHM-1 mutations may differently affect synaptic transmission and short-term synaptic plasticity at different cortical synapses suggests that the neuronal circuits that coordinate and dynamically adjust the balance between excitation and inhibition during cortical activity (Shu et al., 2003) are very likely altered in FHM-1. The specific dominant and efficient role of $Ca_V2.1$ channels in controlling fast neurotransmitter release from central excitatory and inhibitory synapses suggests that the human and mouse $Ca_V2.1$ channelopathies and their episodic neurological symptoms, ranging from migraine to absence epilepsy and ataxia, might primarily be synaptic diseases. The different disorders probably arise from disruption of the finely tuned balance between excitation and inhibition in neuronal circuits of specific brain regions: the cortex in the case of migraine, the thalamus in the case of absence epilepsy and the cerebellum in the case of ataxia. A favored hypothesis considers that the abnormal balance of cortical excitation-inhibition and the resulting persistent state of hyperexcitability of neurons in the cerebral cortex may underlie the increased susceptibility for cortical spreading depression (CSD), which is believed to initiate the attacks of migraine with aura.

Author contributions

1. Conception and design of the experiments: Osvaldo D. Uchitel, Francisco J. Urbano, Carlota Gonzalez Inchauspe.

2. Collection, analysis and interpretation of data: Carlota Gonzalez Inchauspe, Nadia Pilati, Mariano N. Di Guilmi.

3. Writing the paper: Carlota Gonzalez Inchauspe.

4. Revising the paper critically for important intellectual content: Francisco J. Urbano, Nadia Pilati, Osvaldo D. Uchitel, Mariano N Di Guilmi and Ian D Forsythe.

5. Michel D. Ferrari and Arn M.J.M. van den Maagdenberg provided the genetically modified R192Q KI mice.

Acknowledgements

This work was supported by Wellcome Trust grant 084636, UK; ANCyT BID 1728 PICT 2006 N° 199, PICT 2011 N° 2667 and UBACYT X223 Argentina (ODU), as well as by Vici grant 918.56.602 and the Centre for Medical Systems Biology (CMSB) in the framework of the Netherlands Genomics Initiative (NGI). In addition, this work was supported by a grant from FONCYT-Agencia Nacional de Promoción Científica y Tecnológica; BID 1728 OC.AR. PICT-2012-1769 to Dr. Urbano.

We would like to thank María Eugenia Martin for her invaluable technical assistance.

References

Adams, P.J., Rungta, R.L., Garcia, E., van den Maagdenberg, A.M., MacVicar, B.A., Snutch, T.P., 2010. Contribution of calcium-dependent facilitation to synaptic plasticity revealed by migraine mutations in the P/Q-type calcium channel. PNAS 107, 18694–18699.

Akerman, S., Holland, P.R., Goadsby, P.J., 2011. Diencephalic and brainstem mechanisms in migraine. Nat. Rev. Neurosci. 12, 570–584.

Alamilla, J., Gillespie, D.C., 2013. Maturation of calcium-dependent GABA, glycine, and glutamate release in the glycinergic MNTB-LSO pathway. Plos One 8 (9), e75688.

Bahra, A., Matharu, M.S., Buchel, C., Frackowiak, R.S., Goadsby, P.J., 2001. Brainstem activation specific to migraine headache. Lancet 357, 1016–1017.

Brown, S.P., Safo, P.K., Regehr, W.G., 2004. Endocannabinoids Inhibit transmission at granule cell to Purkinje cell synapses by modulating three types of presynaptic calcium channels. J. Neurosci. 24, 5623–5631.

Cao, Y.-Q., Tsien, R.W., 2010. Different relationship of N- and P/Q-type Ca2+ channels to channel-interacting slots in controlling neurotransmission at cultured Hippocampal synapses. J. Neurosci. 30, 4536–4546.

Cao, Y., Aurora, S.K., Nagesh, V., Patel, S.C., Welch, K.M., 2002. Functional MRI-BOLD of brainstem structures during visually triggered migraine. Neurology 59, 72–78.

Cao, Y.Q., Piedras-Renteria, E.S., Smith, G.B., Chen, G., Harata, N.C., Tsien, R.W., 2004. Presynaptic Ca^{2+} channels compete for channel type-preferring slots in altered neurotransmission arising from Ca^{2+} channelopathy. Neuron 43, 387–400.

Eikermann-Haerter, K., Baum, M.J., Ferrari, M.D., van den Maagdenberg, A.M., Moskowitz, M.A., Ayata, C., 2009. Androgenic suppression of spreading depression in familial hemiplegic migraine type 1 mutant mice. Ann. Neurol. 66, 564–568.

Fedchyshyn, M.J., Wang, L., 2005. Developmental transformation of the release modality at the calyx of Held synapse. J. Neurosci. 25, 4131–4140.

Ferrari, M.D., van den Maagdenberg, A.M.J.M., Frants, R.R., Goadsby, P.J., 2008. Migraine as a cerebral ionopathy with impaired central sensory processing. In: Waxman, S.G. (Ed.), Molecular Neurology, pp. 439–461.

Flippen, C., Welch, K.M., 1997. Imaging the brain of migraine sufferers. Curr. Opin. Neurol. 10 (3), 226–230.

Forsythe, I.D., Tsujimoto, T., Barnes-Davies, M., Cuttle, M.F., Takahashi, T., 1998. Inactivation of presynaptic calcium current contributes to synaptic depression at a fast central synapse. Neuron 20, 797–807.

Frank, C.A., Pielage, J., Davis, G.W., 2009. A presynaptic homeostatic signaling system composed of the Eph receptor, ephexin, Cdc42, and $Ca_V2.1$ calcium channels. Neuron 61 (4), 556–569.

Gillespie, D.C., Kim, G., Kandler, K., 2005. Inhibitory synapses in the developing auditory system are glutamatergic. Nat. Neurosci. 8, 332–338.

Giugovaz-Tropper, B., Gonzalez-Inchauspe, C., Di Guilmi, C., Urbano, F.J., Forsythe, I.D., Uchitel, O.D., 2011. P/Q-type calcium channel ablation in a mice glycinergic synapse mediated by multiple types of Ca^{2+} channels alters transmitter release and short-term plasticity. Neuroscience 192, 219–230.

Goadsby, P.J., Lipton, R.B., Ferrari, M.D., 2002. Migraine: current understanding and treatment. N. Engl. J. Med. 346, 257–270.

González Inchauspe, C., Forsythe, I.D., Uchitel, O.D., 2007. Changes in synaptic transmission properties due to the expression of N-type calcium channels at the calyx of held synapse of mice lacking P/Q-type calcium channels. J. Physiol. 584, 835–851.

González Inchauspe, C., Urbano, F.J., Di Guilmi, M.N., Forsythe, I.D., Ferrari, M.D., van den Maagdenberg, A.M., Uchitel, O.D., 2010. Gain-of-function in FHM-1 Ca(V)2.1 knock-in mice is related to the shape of the action potential. J. Neurophysiol. 104 (1), 291–299.

González Inchauspe, C., Urbano, F.J., Di Guilmi, M.N., Ferrari, M.D., van den Maagdenberg, A.M., Forsythe, I.D., Uchitel, O.D., 2012. Presynaptic $Ca_V2.1$ calcium channels carrying familial hemiplegic migraine mutation R192Q allow faster recovery from synaptic depression in mouse calyx of Held. J. Neurophysiol. 108, 2967–2976.

Haerter, K., Ayata, C., Moskowitz, M.A., 2005. Cortical spreading depression: a model for understanding migraine biology and future drug targets. Headache Curr. 2, 97–103.

Hirtz, J.J., Boesen, M., Braun, N., Deitmer, J.W., Kramer, F., Lohr, C., Müller, B., Nothwang, H.G., Striessnig, J., Löhrke, S., Friauf, E., 2011. Cav1.3 calcium channels are required for normal development of the auditory brainstem. J. Neurosci. 31, 8280–8294.

Hirtz, J.J., Braun, N., Griesemer, D., Hannes, C., Janz, K., Lohrke, S., Muller, B., Friauf, E., 2012. Synaptic refinement of an inhibitory topographic map in the auditory brainstem requires functional $Ca_V1.3$ calcium channels. J. Neurosci. 32 (42), 14602–14616.

Iwasaki, S., Takahashi, T., 1998. Developmental changes in calcium channel types mediating synaptic transmission in rat auditory brainstem. J. Physiol. (Lond) 509, 419–423.

Iwasaki, S., Momiyama, A., Uchitel, O.D., Takahashi, T., 2000a. Developmental changes in calcium channel types mediating central synaptic transmission. J. Neurosci. 20, 59–65.

Iwasaki, S., Momiyama, A., Uchitel, O.D., Takahashi, T., 2000b. Developmental changes in calcium channel types mediating central synaptic transmission. J. Neurosci. 20, 59–65.

Joris, P.X., Yin, T.C., 1995. Envelope coding in the lateral superior olive. I. Sensitivity to interaural time differences. J. Neurophysiol. 73, 1043–1062.

Kaja, S., van de Ven, R.C., Broos, L.A., Veldman, H., van Dijk, J.G., Verschuuren, J.J., Frants, R.R., Ferrari, M.D., van den Maagdenberg, A.M., Plomp, J.J., 2005. Gene dosage-dependent transmitter release changes at neuromuscular synapses of CACNA1A R192Q knockin mice are non-progressive and do not lead to morphological changes or muscle weakness. Neuroscience 135, 81–95.

Kaja, S., Van de Ven, R.C.G., Broos, L.A.M., Frants, R.R., Ferrari, M.D., Van den Maagdenberg, A.M.J.M., Plomp, J.J., 2010. Severe and progressive neurotransmitter release aberrations in familial hemiplegic migraine type 1 Cacna1a S218L knock-in mice. J. Neurophysiol. 104, 1445–1455.

Klychnikov, O.I., Li, K.W., Sidorov, I.A., Loos, M., Spijker, S., Broos, L.A., Frants, R.R., Ferrari, M.D., Mayboroda, O.A., Deelder, A.M., Smit, A.B., van den Maagdenberg, A.M., 2010. Quantitative cortical synapse proteomics of a transgenic migraine mouse model with mutated Ca(V)2.1 calcium channels. Proteomics 10 (13), 2531–2535.

Korada, S., Schwartz, I.R., 1999. Development of GABA, glycine, and their receptors in the auditory brainstem of gerbil: a light and electron microscopic study. J. Comp. Neuro l409, 664–681.

Kotak, V.C., Korada, S., Schwartz, I.R., Sanes, D.H., 1998. A developmental shift from GABAergic to glycinergic transmission in the central auditory system. J. Neurosci. 18, 4646–4655.

Lauritzen, M., 1994. Pathophysiology of the migraine aura: the spreading depression theory. Brain 117, 199–210.

Llinas, R., Moreno, H., 1998. Local Ca^{2+} signaling in neurons. Cell. Calcium 24, 359–366.

Luebke, J.I., Dunlap, K., Turner, T.J., 1993. Multiple calcium channel types control glutamatergic synaptic transmission in the hippocampus. Neuron 11, 895–902.

May, A., Goadsby, P.J., 1999. The trigeminovascular system in humans: pathophysiologic implications for primary headache syndromes of the neural influences on the cerebral circulation. J. Cereb. Blood Flow. Metab. 19, 115–127.

Mintz, I.M., Sabatini, B.L., Regehr, W.G., 1995. Calcium control of transmitter release at a cerebellar synapse. Neuron 15, 675–688.

Moore, M.J., Caspary, D.M., 1983. Strychnine blocks binaural inhibition in lateral superior olivary neurons. J. Neurosci. 3, 237–242.

Muller, M., Felmy, F., Schneggenburger, R., 2008. A limited contribution of Ca^{2+} current facilitation to paired-pulse facilitation of transmitter release at the rat calyx of Held. J. Physiol. (Lond) 586, 5503–5520.

Nabekura, J., Katsurabayashi, S., Kakazu, Y., Shibata, S., Matsubara, A., Jinno, S., Mizoguchi, Y., Sasaki, A., Ishibashi, H., 2004. Developmental switch from GABA to glycine release in single central synaptic terminals. Nat. Neurosci. 7, 17–23.

Neher, Sakaba, T., 2001. Combining deconvolution and noise analysis for the estimation of transmitter release rates at the calyx of Held. J. Neurosci. 21, 444–461.

Neher, E., Sakaba, T., 2008. Multiple roles of calcium ions in the regulation of neurotransmitter release. Neuron 59 (6), 861–872.

Ophoff, R.A., Terwindt, G.M., Vergouwe, M.N., van Eijk, R., Oefner, P.J., Hoffman, S.M.G., Lamerdin, J.E., Mohrenweiser, H.W., Bulman, D.E., Ferrari, M., et al., 1996. Familial hemiplegic migraine and episodic ataxia type-2 are caused by mutations in the Ca2+ channel gene CACNL1A4. Cell 87, 543–552.

Pietrobon, D., 2005. Migraine: new molecular mechanisms. Neuroscientist 11, 373–386.

Pietrobon, D., 2010. Cav2.1 channelopathies. Pflugers Arch. - Eur. J. Physiol. 460, 375–393.

Pietrobon, D., Striessnig, J., 2003. Neurobiology of migraine. Nat. Rev. Neurosci. 4 (5), 386–398.

Qian, J., Noebels, J.L., 2000. Presynaptic Ca^{2+} influx at a mouse central synapse with Ca^{2+} channel subunit mutations. J. Neurosci. 20, 163–170.

Reid, C.A., Bekkers, J., Clements, J.D., 1998. N- and P/Q-type Ca^{2+} channels mediate transmitter release with a similar cooperativity at rat hippocampal autapses. J. Neurosci. 18, 2849–2855.

Rosato Siri, M.D., Uchitel, O.D., 1999. Calcium channels coupled to neurotransmitter release at neonatal rat neuromuscular junctions. J. Physiol. 514, 533–540.

Rosato Siri, M.D., Piriz, J., Giugovaz Tropper, B., Uchitel, O.D., 2002. Differential Ca^{2+}-dependence of transmitter release mediated by P/Q- and N-type calcium channels at neonatal rat neuromuscular junctions. Eur. J. Neurosci. 15 (12), 1874–1880.

Sanchez del Rio, M., Alvarez Linera, J., 2004. Functional neuroimaging of headaches. Lancet Neurol. 3 (11), 645–651.

Sanchez-del-Rio, M., Reuter, U., 2004. Migraine aura: new information on underlying mechanisms. Curr. Opin. Neurol. 17 (3), 289–293.
Scheuss, V., Schneggenburger, R., Neher, E., 2002. Separation of presynaptic and postsynaptic contributions to depression by covariance analysis of successive EPCSs at the calyx of held synapse. J. Neurosci. 22, 728–739.
Schneggenburger, R., Meyer, A.C., Neher, E., 1999a. Released fraction and total size of a pool of immediately available transmitter quanta at a calyx synapse. Neuron 23, 399–409.
Schneggenburger, R., Meyer, A.C., Neher, E., 1999b. Released fraction and total size of a pool of immediately available transmitter quanta at a calyx synapse. Neuron 23, 399–409.
Schneggenburger, R., Sakaba, T., Neher, E., 2002a. Vesicle pools and short-term synaptic depression: lessons from a large synapse. Trends Neurosci. 25 (4), 206–212.
Schneggenburger, R., Sakaba, T., Neher, E., 2002b. Vesicle pools and short-term synaptic depression: lessons from a large synapse. Trends Neurosci. 25, 206–212.
Shu, Y., Hasenstaub, A., McCormick, D.A., 2003. Turning on and off recurrent balanced cortical activity. Nature 423, 288–293.
Sterenborg, J.C., Pilati, N., Sheridan, C.J., Uchitel, O.D., Forsythe, I.D., Barnes-Davies, M., 2010. Lateral olivocochlear (LOC) neurons of the mouse LSO receive excitatory and inhibitory synaptic inputs with slower kinetics than LSO principal neurons. Hear Res. 270, 119–126.
Takago, H., Nakamura, Y., Takahashi, T., 2005. G protein-dependent presynaptic inhibition mediated by AMPA receptors at the calyx of Held. Proc. Natl. Acad. Sci. U. S. A. 102, 7368–7373.
Takahashi, T., Momiyama, A., 1993. Different types of calcium channels mediate central synaptic transmission. Nature 366, 156–158.
Takahashi, T., Forsythe, I., Tsujimoto, T., Barnes-Davies, M., Onodera, K., 1996. Presynaptic calcium current modulation by a metabotropic glutamate receptor. Science 274, 594–597.
Taschenberger, H., Leao, R.M., Rowland, K.C., Spirou, G.A., von Gersdorff, H., 2002. Optimizing synaptic architecture and efficiency for high-frequency transmission. Neuron 36, 1127–1143.
Tollin, D.J., 2003. The lateral superior olive: a functional role in sound source localization. Neuroscientist 9, 127–143.
Tottene, A., Conti, R., Fabbro, A., Vecchia, D., Shapovalova, M., Santello, M., van den Maagdenberg, A.M., Ferrari, M.D., Pietrobon, D., 2009. Enhanced excitatory transmission at cortical synapses as the basis for facilitated spreading depression in Cav2.1 knock in migraine mice. Neuron 61, 762–773.
Turrigiano, G., 2012. Homeostatic synaptic plasticity: local and global mechanisms for stabilizing neuronal function. Cold Spring Harb. Perspect. Biol. 4, a005736.
Urbano, F.J., Rosato-Siri, M.D., Uchitel, O.D., 2002. Calcium channels involved in neurotransmitter release at adult, neonatal and P/Q-type deficient neuromuscular junctions (Review). Mol. Membr. Biol. 19, 293–300.
van den Maagdenberg, A.M., Pietrobon, D., Pizzorusso, T., Kaja, S., Broos, L.A., Cesetti, T., van de Ven, R.C., Tottene, A., van der Kaa, J., Plomp, J.J., Frants, R.R., Ferrari, M.D., 2004. A *Cacna1a* Knockin migraine mouse model with increased susceptibility to cortical spreading depression. Neuron 41, 701–710.
van den Maagdenberg, A.M., Haan, J., Terwindt, G.M., Ferrari, M.D., 2007. Migraine: gene mutations and functional consequences. Curr. Opin. Neurol. 20, 299–305.
van den Maagdenberg, A.M., Pizzorusso, T., Kaja, S., Terpolilli, N., Shapovalova, M., Hoebeek, F.E., Barrett, C.F., Gherardini, L., van de Ven, R.C., Todorov, B., Broos, L.A., Tottene, A., Gao, Z., Fodor, M., De Zeeuw, C.I., Frants, R.R., Plesnila, N., Plomp, J.J., Pietrobon, D., Ferrari, M.D., 2010. High cortical spreading depression susceptibility and migraine-associated symptoms in Cav2.1 S218L mice. Ann. Neurol. 67, 85–98.
Vecchia, D., Pietrobon, D., 2012. Migraine: a disorder of brain excitatory-inhibitory balance? Trends Neurosci. 35 (8), 507–520.
von Gersdorff, H., Borst, J.G.G., 2002. Short-term plasticity at the calyx of Held. Nat. Rev. Neurosci. 3, 53–64.
Von Gersdorff, H., Schneggenburger, R., Weis, S., Neher, E., 1997. Presynaptic depression at a calyx synapse: the small contribution of metabotropic glutamate receptors. J. Neurosci. 17, 8137–8146.
Walcher, J., Hassfurth, B., Grothe, B., Koch, U., 2011. Comparative posthearing development of inhibitoryinputs to the lateral superior olive in gerbils and mice. J. Neurophysiol. 106, 1443–1453.
Wang, L.Y., Kaczmarek, L.K., 1998. High frequency firing helps replenish the readily release pool of synaptic vesicles. Nature 394, 384–388.
Weiller, C., et al., 1995. Brain stem activation in spontaneous human migraine attacks. Nat. Med. 1, 658–660.
Welch, M., 1998. The occipital cortex as a generator of migraine aura. Cephalalgia (Suppl 22), 15–21.
Westenbroek, R.E., Hell, J.W., Warner, C., Dubel, S.J., Snutch, T.P., Catterall, W.A., 1992. Biochemical properties and subcellular distribution of an N-type calcium channel a1 subunit. Neuron 9, 1099–1115.
Westenbroek, R.E., Hoskins, L., Catterall, W.A., 1998. Localization of Cav2.1 channel subtypes on rat spinal motor neurons, interneurons, and nerve terminals. J. Neurosci. 18, 6319–6330.
Wong, A.Y.C., Graham, B.P., Billups, B., Forsythe, I.D., 2003. Distinguishing between presynaptic and postsynaptic mechanisms of short-term depression during action potential trains. J. Neurosci. 23, 4868–4877.
Wu, L.G., Borst, J.G.G., 1999. The reduced release probability of releasable vesicles during recovery from short-term synaptic depression. Neuron 23, 821–832.
Wu, L.G., Saggau, P., 1997. Presynaptic inhibition of elicited neurotransmitter release. Trends Neurosci. 20 (5), 204–212.
Wu, L.G., Westenbroek, R.E., Borst, J.G.G., Catterall, W.A., Sakmann, B., 1999. Calcium channel types with distinct presynaptic localization couple differentially to transmitter release in single calyx-type synapses. J. Neurosci. 19, 726–736.
Xu, J., Wu, L.G., 2005. The decrease in the presynaptic calcium current is a major cause of short-term depression at a calyx-type synapse. Neuron 46, 633–645.
Yang, Y.M., Wang, L.Y., 2006. Amplitude and kinetics of action potential-evoked Ca2+ current and its efficacy in triggering transmitter release at the developing calyx of Held synapse. J. Neurosci. 23, 5698–5708.
Zucker, R.S., Regehr, W.G., 2002. Short-term synaptic plasticity. Ann. Rev. Physiol. 64, 355–405.